Journal of Histochemistry & Cytochemistry 1–14

DOI: 10.1369/00221554251374732
journals.sagepub.com/home/jhc
Sage

Alterations in Inflammatory Markers and Tissue Architecture in the Gerbil Prostate Following Castration

Nayara Fernanda Costa Castro, Vitor Grigio, Cássia Regina Suzuki Caires, Mariele Ilario Zucão, Sebastião Roberto Taboga, and Patrícia Simone Leite Vilamaior

Department of Biological Sciences, Institute of Biosciences, Humanities and Exact Sciences, São Paulo State University (UNESP), São Paulo, Brazil (NFCC, VG, CRSC, MIZ, SRT, PSLV)

Summary

Orchiectomy induces atrophy of epithelial cells in the prostate gland, stimulated by androgen deprivation. The objective of the current study was to assess the changes arising from tissue remodeling during short periods of androgen deprivation in the ventral prostate of Mongolian gerbils. Adult male gerbils were divided into groups: control and castrated, euthanized on the 3rd (Ca3d), 7th (Ca7d), and 14th (Ca14d) days post-orchiectomy (n = 7/group). The ventral lobe of the prostate was submitted for histological, stereological, morphometric, serological, and immunohistochemical analyses. Castration promoted a reduction in the weight of the ventral prostate. It altered the relative proportion of prostate tissue compartments, such as a decrease in the epithelium and non-muscular stroma and an increase in the muscular stroma. In addition, we observed that the number of Cd-68 positive cells increased in the Ca3d group, which represents a period of androgen deprivation not previously reported in the literature for Mongolian gerbils. Matrix metalloproteinase-9 quantification revealed a decrease in the Ca7d group compared to the Ca3d. In addition, the frequency of Tumor Necrosis Factor alpha increased in the Ca14d group, influenced by the duration of testosterone deficiency. The findings contribute to the understanding of prostate tissue remodeling after castration, as well as highlighting the rapid alterations in the prostate microenvironment in a short period following castration: **(J Histochem Cytochem XX: XXX–XXX, XXXX)**

Keywords

androgen deprivation, cytokines, macrophages, orchiectomy, testosterone, tissue remodeling

Introduction

Androgen deprivation therapies are highly applicable in cases of prostate cancer.[1–3] Androgens play a regulatory role in the pathogenesis of prostate cancer through androgen receptors (AR).[4] Androgen deprivation alters AR levels, mediating the epithelial-mesenchymal transition of the prostate and interfering with the development of prostate cancer.[5] It is estimated that approximately 50% of patients diagnosed with prostate cancer will receive androgen deprivation as a treatment.[6–9] This process can occur through chemical or surgical castration (orchiectomy), which results in the suppression of testicular androgen levels.[1] Studies indicate that orchiectomy, associated

Received for publication March 11, 2025; accepted August 18, 2025.

Corresponding Author:
Patrícia Simone Leite Vilamaior, Department of Biological Sciences, Institute of Biosciences, Humanities and Exact Sciences, São Paulo State University (UNESP), Rua Cristóvão Colombo, 2265, Jardim Nazareth, São José do Rio Preto, São Paulo 15054-000, Brazil.
E-mail: patricia.vilamaior@unesp.br

with the administration of antiandrogenic drugs, is an effective therapy for benign prostatic hyperplasia and prostate cancer.[10,11]

Although testosterone (T) is the primary circulating plasma androgen in the prostate, the predominant androgen is the hormone dihydrotestosterone (DHT), formed from T by the action of the enzyme 5α-reductase.[12] T and DHT bind to the same type of receptor, the androgen receptor (AR), but cause different physiological effects.[13] In addition to these hormones, other androgenic hormones are present in the organism, including Dehydroepiandrosterone (DHEA) and Sulfate-Dehydroepiandrosterone (SDHEA), two precursors of steroid hormones produced by the adrenal glands that are converted into androgens in peripheral tissues, such as the prostate.[14-17] The adrenal glands are responsible for the production of approximately 5% of T,[12] which remains circulating through the body even after the removal of the testicles. However, this percentage of T is insufficient to assure homeostasis in the epithelium and prostatic stroma.[18]

After castration, the prostatic epithelium regresses and smooth muscle cells (SMCs) start to adapt to the stromal compartment.[19,20] This adaptive process reduces the activity of epithelial structures and leads to a reduction in the secretion present in the lumen.[21,22] Furthermore, SMCs play an important role in inducing epithelial death by releasing death signals from stromal cells or inhibiting the production of survival factors.[22–24] Epithelial atrophy occurs due to apoptosis of these cells in the face of hormonal ablation.[22] This cell death process is related to the recruitment of lymphocytes, mast cells, and macrophages[25–27] and is signaled by the action of TNF-α (tumor necrosis factor alpha).[28] In addition to alterations in the prostate epithelium, the prostate stroma can undergo remodeling caused by androgen deprivation.[29] These alterations may be related to matrix metalloproteinases (MMPs) such as MMP-2 and MMP-9. These enzymes can degrade components of the extracellular matrix, such as collagen, elastin, and proteoglycans, and cause rearrangement of the stroma.[30]

The use of experimental models, such as the Mongolian gerbil, to understand the relationships between the tissue compartments has allowed clarification of the responses of the prostate to different conditions.[31–34] These studies allow us to expand the knowledge on the histophysiology of this gland, which is of great importance for homeostasis and functionality of the male genital system. Therefore, the current study aimed to analyze the process of tissue remodeling of the ventral prostate of gerbils in different periods of androgen deprivation, with a focus on understanding the role of some cellular components in the prostate stroma and epithelium.

Material and Methods

Animals

To perform this study, 28 adult male gerbils (*Meriones unguiculatus*) (3 months of age) were maintained in the Animal Breeding Center of the Institute of Biosciences, Humanities and Exact Sciences (IBILCE) of the São Paulo State University (UNESP) in polyethylene cages, with a wood shaving substrate, under controlled conditions of luminosity and temperature (23ºC), being provided with filtered water and rodent food ad libitum. The experiments were conducted according to the standards defined by the National Council for the Control of Animal Experimentation (CONCEA, Brazil), and the procedures were approved by the Ethics Committee on the Use of Animals at IBILCE/UNESP (protocol number 123/2015).

Experimental Design

Male Mongolian gerbils were divided into groups (n = 7): control intact (C) and castrated (Fig. 1). When the animals reached 90 days of age, the castrated group was anesthetized to perform the orchiectomy with 1 ml/kg of the solution containing Ketamine and Xylazine, in the proportion of 10:3, respectively. The animals were then maintained under observation and euthanized on the 3rd (Ca3d), 7th (Ca7d), or 14th (Ca14d) day after castration, each of these days representing a group of the castrated animals. Each group had seven animals, totaling 28 animals, and no animals died during the experiment. The animals in the control group were euthanized at the end of the experiment (104 days of age).

Biometric Analysis

On the day of euthanasia, all animals received an overdose of anesthetic (three times the dose used for surgery) administered subcutaneously. They were then weighed and euthanized by decapitation. We collected the body blood (through the rupture of cervical vessels), adrenal glands, and prostate complex. The prostate complex was weighed with all lobes. The ventral prostate was separated and weighed. The relative weights of the prostate complex and ventral prostate were calculated as a proportion by dividing the organ weight by the body weight.

The ventral prostate was fixed in 4% paraformaldehyde, dehydrated in ethanol, clarified in xylol, and then included in Histosec (Merck, Germany). The ventral lobe of the prostate was sectioned at 4 µm and stained by the histochemical techniques Gömori's Reticulin (to identify the reticular fibers of

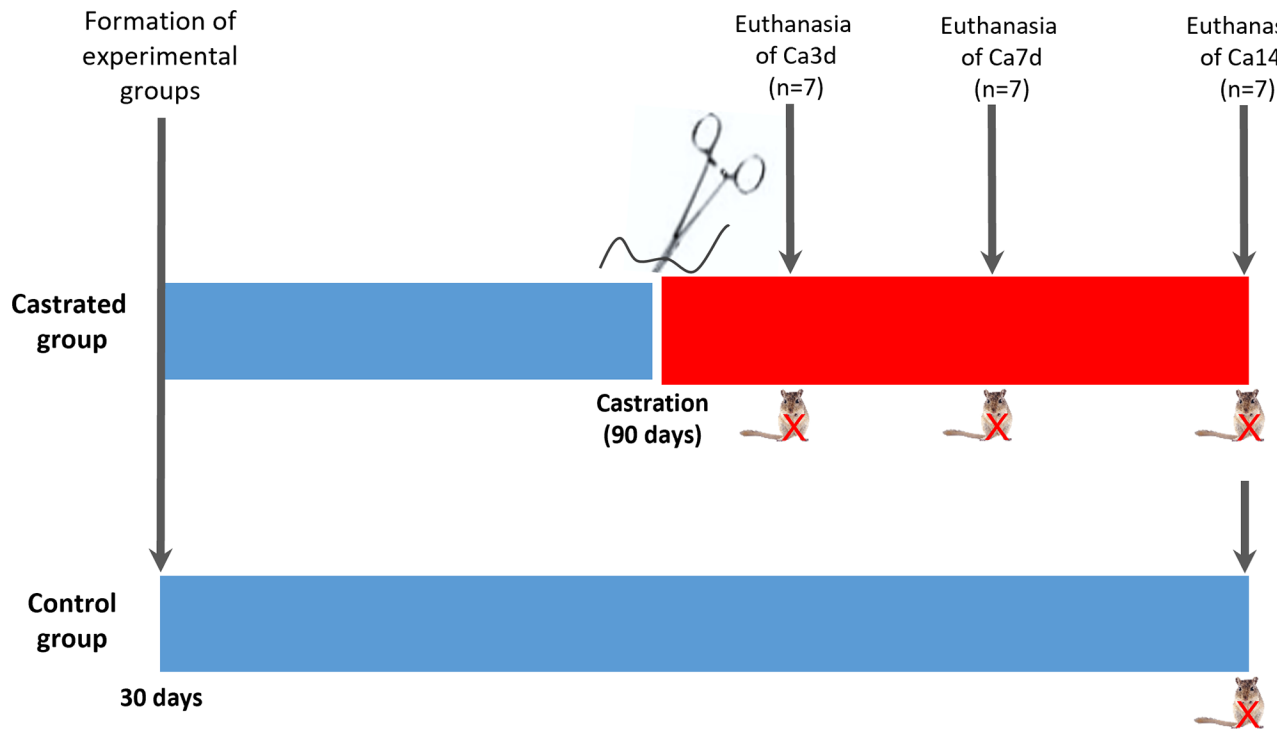

Figure 1. Schematic of the experimental design of the Control and Castrated groups (Ca3d, Ca7d, and Ca14d).

the prostatic stroma) and Gömori's Trichrome (to identify the SMCs and collagen).

Stereological and Morphometric Analysis

Stereological analyses were performed on slides stained with Gömori's Trichrome to obtain the relative volume of the different prostatic compartments. In total, 35 random fields (5 fields for each animal in each group, n = 7) were digitized with a BX61VS camera (Olympus Corporation, Tokyo, Japan) coupled to an Olympus VS120 Virtual Microscopy Slide Scanning System (*VS120-S5*) at 200× magnification for stereological analysis and at 1000× magnification for morphometric analysis, using the same light intensity. To avoid bias in the analyses, the entire slide was photographed and then, using randomization software, the five fields from each slide that were analyzed were randomly selected. A histological section of the medial region of the ventral prostate was selected so that all regions of the organ would be represented.[32] The measurements were obtained according to the M130 multipoint test system proposed by Weibel (1978),[35] and applied to the prostate by Huttunen and collaborators (1981),[36] using Image Pro-Plus 6.0 software (Media Cybernetics, Inc., MD). Using Weibel's method, the relative frequency of each compartment was then quantified in each field, taking into account the following characteristics: epithelial (glandular epithelial cells) and luminal compartments (space surrounded by glandular epithelium that stores the secretion product), muscular stroma (region surrounding the epithelium and formed by smooth muscle tissue), non-muscular stroma (region of the stroma that does not contain SMCs, formed by connective tissue and rich in extracellular matrix fibers and including the nerves), and blood vessels (all arteries and veins included in their lumens) of the ventral prostate were calculated. The quantification of collagen fibers in the tissue was also performed using Weibel's M130 multipoint test, mentioned above, using histological sections stained with Gömori's reticulin.

Morphometry was also performed to obtain the height/thickness of the epithelial cells and the layer of SMCs, respectively. In this analysis, 210 measurements were obtained per group (6 fields/animal, n = 7). The slides were stained by the Gömori's Trichrome. They were digitized with a BX61VS camera (Olympus Corporation, Tokyo, Japan) coupled to an Olympus VS120 Virtual Microscopy Slide Scanning System (*VS120-S5*), with the Image program Pro-Plus (Media Cybernetics).

Serum Hormone Level

Hormonal measurements were determined by ELISA using a high-sensitivity kit for T (Monobind Inc. Lake

Forest, CA) and SDHEA (IBL International, Hamburg, Germany—items number 52151 and number 5204) following the manufacturer's instructions. The reading was performed in a microplate reader (Epoch Multi-Volume Spectrophotometer; System-BioTek Instruments, VT, and TECAN—Infinite F50).

Immunohistochemical Analysis

The primary antibodies used were: anti-Androgen Receptor (AR, rabbit polyclonal IgG, N-20, sc-816; Santa Cruz Biotechnology, Santa Cruz, CA, 1:75 dilution), anti-Cd-68 (goat polyclonal IgG M-20, sc-7084; Santa Cruz Biotechnology, 1:50 dilution), anti-Cd-163 (rabbit polyclonal IgG M-96, sc-33560; Santa Cruz Biotechnology, 1:50 dilution), anti-MMP-2 (monoclonal mouse, sc-13595; Santa Cruz Biotechnology, 1:50 dilution), anti-MMP-9 (monoclonal mouse, sc-21733; Santa Cruz Biotechnology, 1:50 dilution), and anti-TNF-α (rabbit monoclonal IgG, D2D4, XP, # 11948; Cell Signaling, Danvers, MA, 1:75 dilution). Antigen retrieval was performed in pH 6.0 citrate buffer at 92C for 45 min. The blocking of endogenous peroxidases was performed with 3% H2O2 for 15 min and nonspecific protein reactions were blocked with 5% skimmed milk in TBSt for 30 min (for the AR, Cd-68, MMP-2, MMP-9 and TNF-α protocols) and 60 min (for the Cd-163 protocol). Histological sections were incubated with primary antibodies overnight at 4ºC. Subsequently, they were incubated with secondary antibodies labeled with peroxidase (AR, Cd-68, Cd-163 protocols: rabbit ABC Staining System SC-2018; Santa Cruz Biotechnology) or polymer (MMP-2, MMP-9, TNF-α protocol: DAKO EnVision, Dual Link System-HRP, Dako, CA) for 40 min at 22°C. Immunoreactive staining was detected by diaminobenzidine (DAB; Sigma, St. Louis, MO) for approximately 30 seconds and counterstained with Harris Hematoxylin. The slides were then dehydrated in ethanol, clarified, and mounted on Canadian balsam and evaluated using conventional light microscopy.

The relative frequency of AR-positive epithelial and stromal cells was obtained from the count of 4000 cells in each compartment, per experimental group, in serial sections (n = 7) and calculated as the percentage of immunoreactive cells. In addition, the absolute frequency of immunoreactivity for Cd-68 (n = 7), Cd-163 (n = 7), and TNF-α (n = 5) was measured, counting all immunoreactive cells present in the histological section. The expression of MMP-2 and MMP-9 by optical density (OD) (n = 5) was also determined. The images were captured using the Olympus BX60 photomicroscope and the slide scanner (Olympus BX-UCB). The software Image-Pro-Plus (Average Cybernetics) and Image J with plugin IHC profiler[37] were used to count the number of immunoreactive cells and to quantify the intensity of immunostaining, respectively.

Immunofluorescence

The histological slides were subjected to immunofluorescence for the detection of muscle fibers by α-actin (monoclonal mouse IgG2a, sc-32251; Santa Cruz Biotechnology, dilution 1:100). Antigen retrieval was performed in pH 6.0 citrate buffer at 92C for 50 min. Nonspecific proteins were blocked using 5% skimmed milk in PBS (phosphate buffer solution) for 60 min, followed by incubation with the primary antibody (anti-α-actin) at 4C, overnight. The material was incubated in a secondary anti-mouse antibody, containing the fluorochrome FITC (Fluorescein isothiocyanate) (sc-2010; Santa Cruz Biotechnology, dilution 1:200) for 2 hr. An appropriate mounting medium containing DAPI (Ultracruz Mounting Medium: sc-24941, for fluorescence with DAPI; Santa Cruz Biotechnology) was used. The images were analyzed using a Zeiss Axio Imager M2, Zeiss fluorescence microscope, Zeiss (Gottingen, Germany).

Statistical Analysis

The statistical analysis was performed with spreadsheets and graphs using GraphPad Prism 6.00 software. The data were subjected to the Kolmogorov-Smirnov test to analyze the normality of the distribution. Quantitative analysis was based on parametric (analysis of variance; ANOVA) and nonparametric (Kruskal-Wallis) tests, followed by Tukey and Dunn multiple comparison tests, respectively. Differences were considered statistically significant when $p<0.05$.

Results

The Prostate Weight Reduced After Orchiectomy in the Gerbils

The biometric data show no differences in body weight when comparing the control group with the castrated groups (Table 1). However, the analysis of the relative weight of the prostate complex revealed a significant reduction in the Ca7d and Ca14d groups in comparison to Ca3d and Ca14d compared to the control group. The Ca3d group shows no statistical differences compared to the control group (Table 1). Analysis of the weight of the ventral prostate demonstrated a reduction in the castrated groups compared to the C group

Table 1. Biometric, Stereological and Morphometric Parameters of Mongolian Gerbils in the Experimental Groups.

Parameters	Experimental groups			
	Control	Ca3d	Ca7d	Ca14d
Biometric data (n = 7)				
Body weight (g)	71.43 ± 5.85	67.43 ± 4.72	73.43 ± 5.74	74.57 ± 5.38
Prostatic complex weight (mg)	604.4 ± 45.38[a]	627.0 ± 62.74[a]	316.8 ± 53.55[a,b]	158.0 ± 42.60[b]
Prostatic complex relative weight ($\times 10^{-3}$)	8.47 ± 0.42[a,b]	9.33 ± 1.14[a]	4.35 ± 0.93[b,c]	2.10 ± 0.53[c]
Ventral lobe weight (mg)	28.81 ± 17.31[a]	10.34 ± 5.24[b]	12.40 ± 5.38[b]	7.42 ± 6.18[b]
Ventral lobe relative weight ($\times 10^{-4}$)	3.86 ± 2.50[a]	1.53 ± 0.76[a,b]	1.67 ± 0.68[a,b]	0.97 ± 0.78[b]
Adrenal (g)	0.033 ± 0.005	0.036 ± 0.004	0.037 ± 0.007	0.038 ± 0.003
Stereological data (%)				
Epithelium	17.84 ± 7.65[a]	17.88 ± 7.95[a]	12.89 ± 5.05[b]	22.52 ± 9.73[a,b]
Lumen	53.52 ± 13.34[a]	52.60 ± 15.68[a,b]	57.07 ± 16.94[a]	44.53 ± 13.82[b]
Muscle stroma	8.22 ± 2.87[a]	10.12± 3.58[a]	10.44 ± 5.96[a]	14.08 ± 5.70[b]
Non-muscle stroma	15.46 ± 9.45[a]	14.54 ± 11.22[a]	6.63 ± 6.00[b]	15.47 ± 7.98[a]
Collagen	1.80 ± 1.35[a]	2.67 ± 2.11[a]	8.18 ± 4.63[b]	6.61 ± 3.75[b]
Blood vessels	2.60 ± 2.33[a]	1.26 ± 1.33[b]	1.11 ± 1.38[b]	1.55 ± 1.74[a,b]
Morphometric data (µm)				
Epithelium	13.30 ± 4.72[a]	9.80 ± 3.72[b]	8.63 ± 2.74[c]	9.71 ± 3.14[b]
Muscle stroma	8.51 ± 3.75[a]	7.47 ± 3.07[b,c]	7.07 ± 2.63[b]	7.77 ± 2.60[a,c]

Data was expressed as mean ± standard deviation.
Statistically significant differences ($p \leq 0.05$) are represented by [a, b, c].

(Table 1). We did not find differences between the weights of the adrenal glands in the different experimental groups (Table 1).

Stereology and Morphometry Analyses Showed a Reduction in the Proportion of Prostate Compartments in the Castrated Groups

Stereological analyses quantification revealed a decrease in the epithelial compartment in the Ca7d group compared to C and Ca3d, and there was no difference in the Ca14d group. We also verified a decrease in the relative volume of the lumen in the Ca14d group in comparison to C and Ca7d and there were no changes in the Ca3d group. However, analysis of the relative volume of the muscular stroma showed an increase in Ca14d compared to the other groups. The Ca7d group presented a decrease in the non-muscular stroma compared to the other groups. We also observed an increase in the relative volume of collagen in Ca7d and Ca14d compared to the C and Ca3d groups. The Ca3d and Ca7d groups presented a reduction in the relative volume of blood vessels compared to the C group (Table 1).

The morphometric analysis showed differences in the height of the epithelial cells and the thickness of the muscular stroma between the C and castrated groups. We observed a decrease in epithelial height in all castrated groups compared to C and in Ca7d compared to Ca3d and Ca14d. We also verified a decrease in the thickness of the muscular stroma cells in the Ca3d and Ca7d groups compared to C, and in Ca7d compared to the Ca14d group (Table 1).

Castration Altered the Distribution of Reticular and Collagen Fibers, and the SMCs

The morphological analysis revealed an apparent increase in the proportion of reticular and collagen fibers distributed at random, presenting different organizations in the Ca7d and Ca14d groups compared to the control group (Fig. 2H, K). In addition, the immunofluorescence for SMCs demonstrated changes in the distribution of these cells in the muscular stroma in the castrated groups mainly in the Ca14d group, which showed more sparse cells and more intense staining (Fig. 2C, F, I, L, M).

Castration Altered the Serum Levels of T, but not of SDHEA

The decline in circulating testosterone levels in castrated animals can be seen as early as day 3 compared to the control. In addition, a decline was observed in groups Ca7d and Ca14d compared to the control. However, when comparing testosterone levels among the three castrated groups, there was no difference between them (Fig. 3A). We did not observe differences in SDHEA dosage (Fig. 3B).

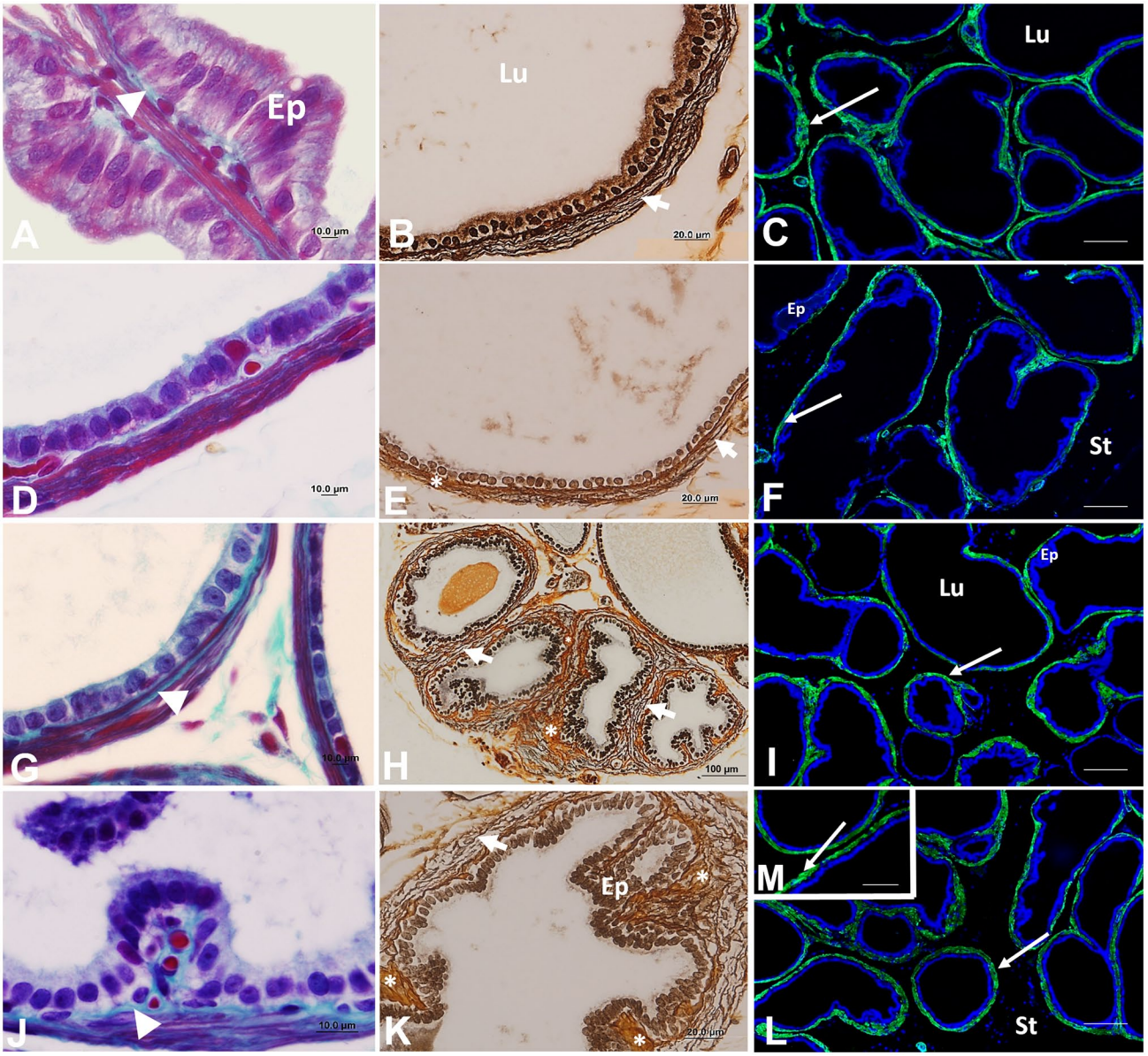

Figure 2. Histological sections of the ventral prostate of gerbils stained by Gömori's trichrome (A, D, G, J) and Gömori's reticulin (B, E, H, K) and subjected to α-actin immunofluorescence (C, F, I, L, M) showing the alterations caused by the orchiectomy in the ventral prostate. Control Group (A-C), non-castrated animals. Castrated groups were euthanized after 3 (Ca3d) (D-F), 7 (Ca7d) (G-I), and 14 days (Ca14d) (J-L). Epithelium (Ep), Lumen (Lu), stroma (St), smooth muscle cell layer (SMC), blue collagen fibers (arrowhead), reticular fibers (short arrows), collagen fibers (asterisk), smooth muscle in fluorescent green (long arrows). Scale bar 10µm (A, D, G, J), 20µm (B, E, H, K) and 100µm (C, F, I, L, M).

Immunohistochemistry Analyses Showed an Increase in AR-Positive Cells, Macrophages, and TNF-α-Positive Cells and a Decrease in the MMP-9 Enzyme

We first performed immunohistochemistry to detect the androgen receptor (AR) in the nucleus of prostatic epithelial and stromal cells in all experimental groups (Fig. 4A–F). We verified an increase in AR-positive cells in both prostatic compartments of the castrated groups, especially in the Ca3d and Ca14d animals (Fig. 4G). However, we observed a decrease in these immunoreactive cells in the epithelium of Ca7d animals when compared to the Ca3d group (Fig. 4G).

We next evaluated the tissues for Cd-68 immunostaining, which revealed the presence of pan macrophages in the epithelial and stromal compartments in all experimental groups (Fig. 5A–F). Ca3d animals presented an increase in Cd-68 positive cells in the epithelium, while there were no significant changes in

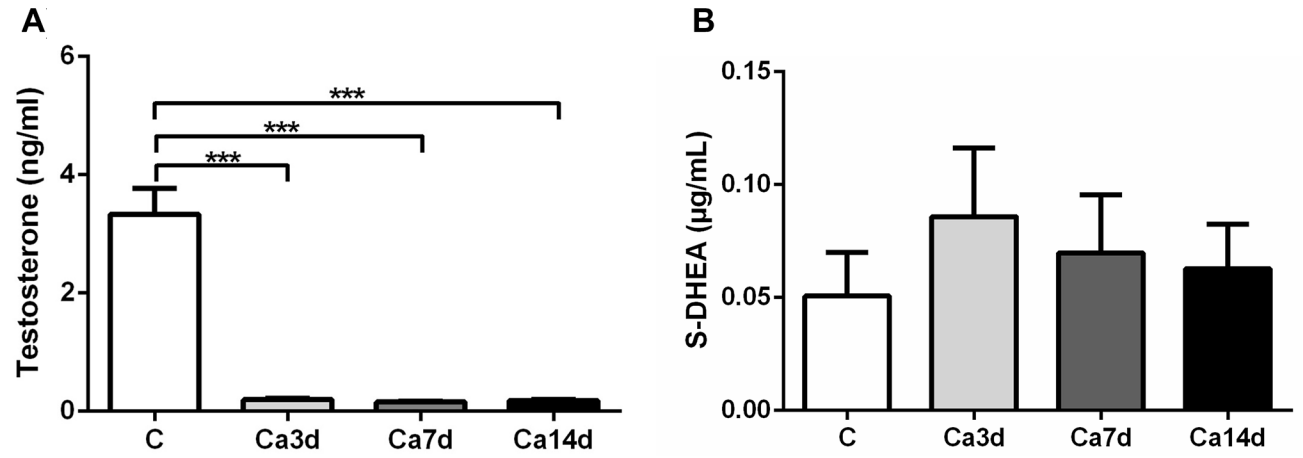

Figure 3. Orchiectomy alters the serum hormone levels of testosterone (A), but not of SDHEA (B). Statistical analyses were based on one-way ANOVA followed by Tukey (post hoc). ***$p<0.001$. Control group (C) and castrated groups were euthanized at 3 (Ca3d), 7 (Ca7d), and 14 (Ca14d) days after the orchiectomy.

the stroma. (Fig. 5 O). We also checked for the presence of Cd-163-positive macrophages in the stroma and in the prostatic intraepithelial region (Fig. 5G–N). However, we did not observe significant differences in the number of these cells among the experimental groups (Fig. 5P).

The distribution of MMP-2 and MMP-9 was evaluated in the prostatic compartments (Fig. 6A–J). The MMP-2 frequency did not demonstrate differences (Fig. 6K). However, we verified a decrease in MMP-9 in the Ca7d group compared to Ca3d (Fig. 6L). Finally, we investigated the frequency of TNF-α-positive cells in the tissue compartments of the ventral prostate (Fig. 7A–E), and we observed an increase in Ca14d animals compared with the C and Ca3d groups (Fig. 7F).

Discussion

The androgens influence the remodeling of the prostate gland after orchiectomy[26,38,39] and alter the balance between cell proliferation and death in the prostatic tissue compartments.[18,22,40] That said, we thus proposed to analyze the process of tissue remodeling of the ventral prostate of Mongolian gerbils in different periods of androgen ablation. The castration altered the distribution of the ventral prostate compartments and the frequency of androgen receptors, macrophages, MMPs, and TNF-α, promoting tissue reorganization.

The results showed a reduction in the relative volume of epithelial cells after 7 days of hormone deprivation. There was also a decrease in the height of the ventral prostate epithelium in all castrated groups. The epithelial alterations were related to a decrease in secretory activity (such as the elimination of accumulated secretions, and reduced functions of the endoplasmic reticulum and Golgi complex) and loss of epithelial cells via apoptosis, one of the factors that causes atrophy of the prostate gland.[23,38] This atrophy is consistent with the results of the biometric analysis, which showed the influence of this hormonal ablation on the relative weight of the prostate complex and the ventral prostate in the castrated groups. Our results are consistent with Góes et al. (2007), who reported that the ventral lobe of the gerbil prostate is more responsive to the condition of androgen deprivation in a short period (7 days). The atrophy of the prostate epithelium in the face of androgen deprivation is related to the regulatory role that testosterone and DHT play in this gland. Testosterone is converted into DHT in the prostate and regulates the secretory function of the prostate, as well as the size of the prostate and its compartments.[41,42]

The morphometric analysis showed a decrease in the thickness of the muscular stroma in the castrated groups compared to the control group. This process can be caused by reducing the expression of some critical components, such as contractile proteins, which act in the contraction process. Cellular atrophy is characterized by the accumulation of large lipofuscin granules in the cytoplasm and the decrease in cell volume.[18] This atrophic process has also been observed in telocytes, cells associated with the epithelium and smooth muscle, which presented alterations in their phenotype in the face of orchiectomy.[20] Studies indicate that SMCs have active androgen receptors and, with fibroblasts, are important elements in stromal reorganization after castration.[18,43] However, when analyzing the relative

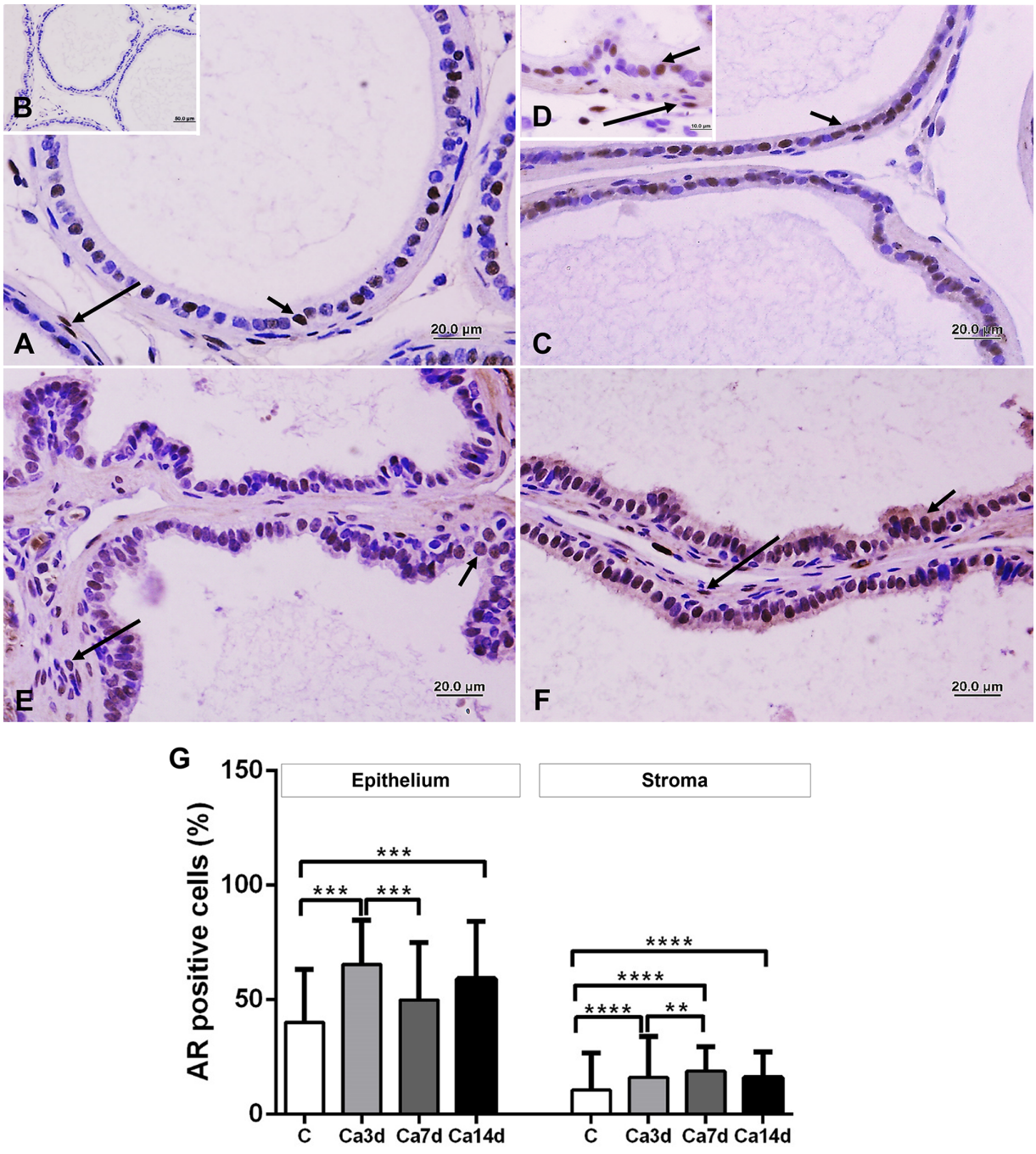

Figure 4. Frequency of androgen receptor (AR)-positive cells increased in the castrated animals. Negative reaction control (B) slides were not incubated with primary antibody. Control (A), non-castrated animals. Castrated groups were euthanized at 3 (Ca3d) (C, D), 7 (Ca7d) (E), and 14 (Ca14d) (F) days after the orchiectomy. AR positive cells are indicated in the epithelial compartment by smaller arrows and in the stromal compartment by larger arrows. The data represent averages of the relative frequency (%) of AR-positive cells and the error bars indicate the standard deviation. **, *** and **** indicate statistically significant differences ($p<0.01$; $p<0.001$; and $p<0.0001$ respectively), according to the Kruskal-Wallis test followed by the post hoc Dunn test (G). Scale bar 20µm.

volume of tissue compartments, muscle stroma increased in the Ca14d group in comparison to C. This increase in the stroma could indicate that although there is a decrease in the thickness of the muscular stroma, the decrease in the height of epithelial cells, indicates that, in the proportion between the compartments, the muscular stroma occupies greater volume in the condition of the remodeled gland after the

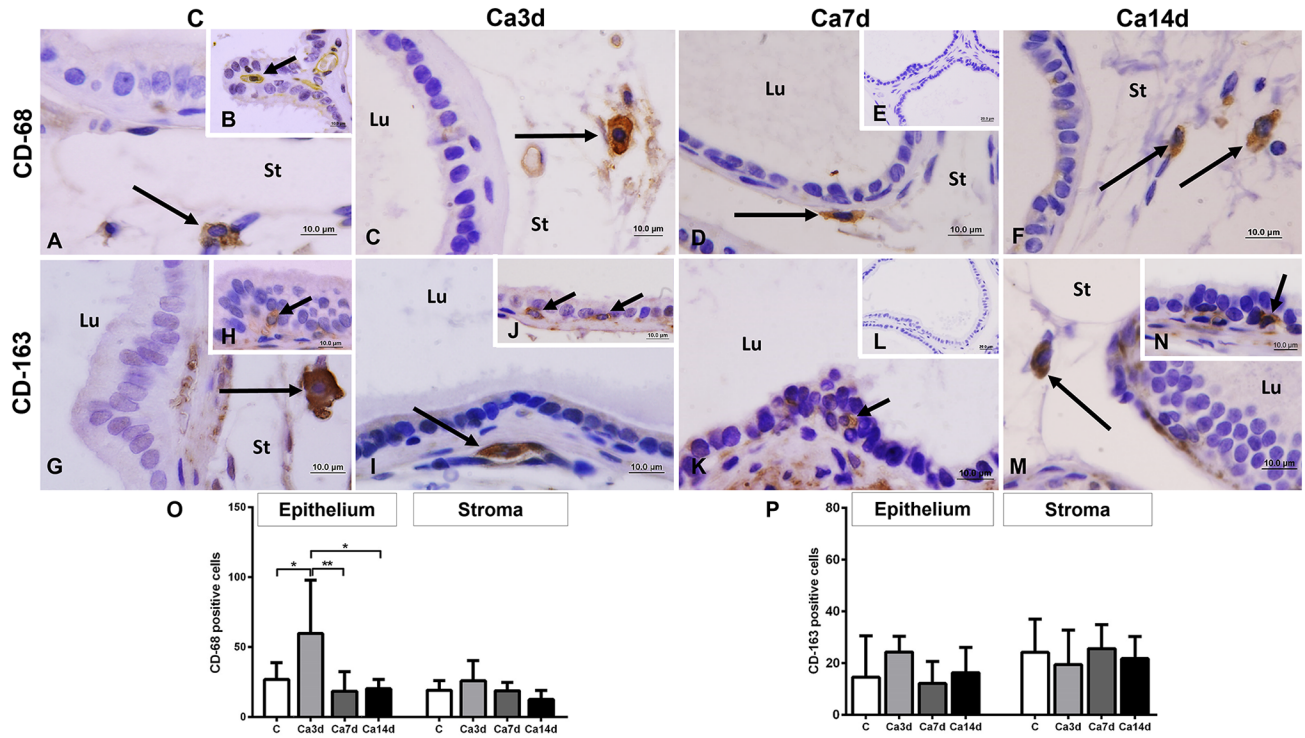

Figure 5. Castration alters the distribution of Cd-68, but not of Cd-163 macrophages. Negative reaction controls (E, L), that were not incubated with primary antibodies (Cd-68 and Cd-163). Controls (A, B, G, H), non-castrated animals. Castrated groups were euthanized at 3 (Ca3d) (C, I, J), 7 (Ca7d) (D, E, K, L), and 14 (Ca14d) (F, M, N) days after the orchiectomy. Intraepithelial macrophages are indicated by small arrows, and stromal macrophages by large arrows. The data represent averages of the number of macrophages by histological section marked with the anti-Cd-68 (O) and anti-Cd-163 (P) antibodies, and the error bars indicate the standard deviation. * and ** indicate statistically significant differences ($p<0.05$ and $p<0.01$, respectively), according to the Kruskal-Wallis test followed by the post hoc Dunn test (O). The data in (P) were tested via one-way ANOVA, followed by the post hoc Tukey test. St, stroma; Lu, lumen. Scale bar 10μm.

orchiectomy. Previous studies observed this same process was during different castration periods.[10,19]

Smooth muscle cell is directly associated with collagen fibers, and this association may indicate that these fibers play an active role in the reorganization of the extracellular matrix due to the involution of epithelial structures after androgen depletion.[44] Our results are consistent with these observations and indicate that castration results in significant reorganization of the collagen and reticular fibers, which are more dispersed in the Ca7d and Ca14d groups.

Analysis of serum T levels showed a decrease in circulating T in animals submitted to orchiectomy, as already observed in many studies.[14,15,23,45] Research indicates that, in humans, the concentration of androgens present in the organism reduces by approximately 59% after orchiectomy. However, 41% of these hormones are still present in the body even after the elimination of testicular androgens.[15] Other studies have observed that 50% of DHT remained in the prostate of orchiectomized patients.[46] Thus, we observed a tendency to an increase in the serum levels of SDHEA in the castrated groups in comparison to C, mainly in Ca3d. These results indicate that the production of androgens remains active through the synthesis of these hormones in peripheral tissues and by greater activity of the adrenal glands, even after castration.

The hormonal alterations also affected androgen receptor expression. Many studies show that after castration, the expression of AR decreases, mainly in the ventral lobe of the rodent prostate.[40,45,47] However, some studies report that around 24 to 48 hr after surgical castration, this decrease does not occur.[47–49] Our results corroborate this information, as there was also no reduction in the frequency of AR in the ventral prostate. The increase in these receptors can occur as a strategy, considering the dependence on androgens, for the maintenance of the gland, to avoid or delay the atrophy process. Husmannt and collaborators (1990) demonstrated that, in rats, most ARs are present in the nucleus of prostate cells from intact and castrated animals.[47] Thus, the authors suggest that the AR remains in the nucleus even in the absence of ligands. Furthermore, this increase in AR after castration can be

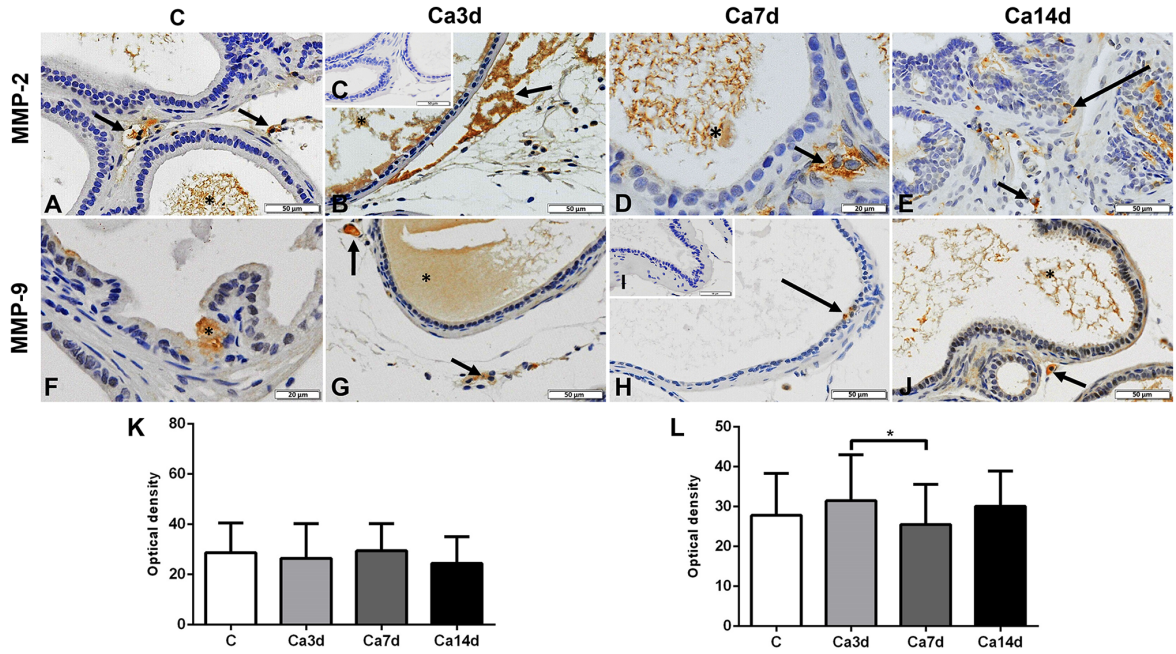

Figure 6. The immunohistochemistry shows the distribution of MMPs in the ventral prostate of all groups. Negative reaction controls (C, I), that were not incubated with primary antibodies. Control (A, F), non-castrated animals. Castrated groups were euthanized at 3 (Ca3d) (B, C, G), 7 (Ca7d) (D, H, I), and 14 (Ca14d) (E, J) days after the orchiectomy. Positive staining in the epithelium and stroma (arrows) and the secretion present in the lumen (asterisk). The data represent averages of the quantification of the immunostaining intensity by optical density (OD) and the error bars show the standard deviation (K, L). * indicates a statistically significant difference ($p<0.05$), according to the Kruskal-Wallis test followed by the post hoc Dunn test (L). Scale bar 50µm.

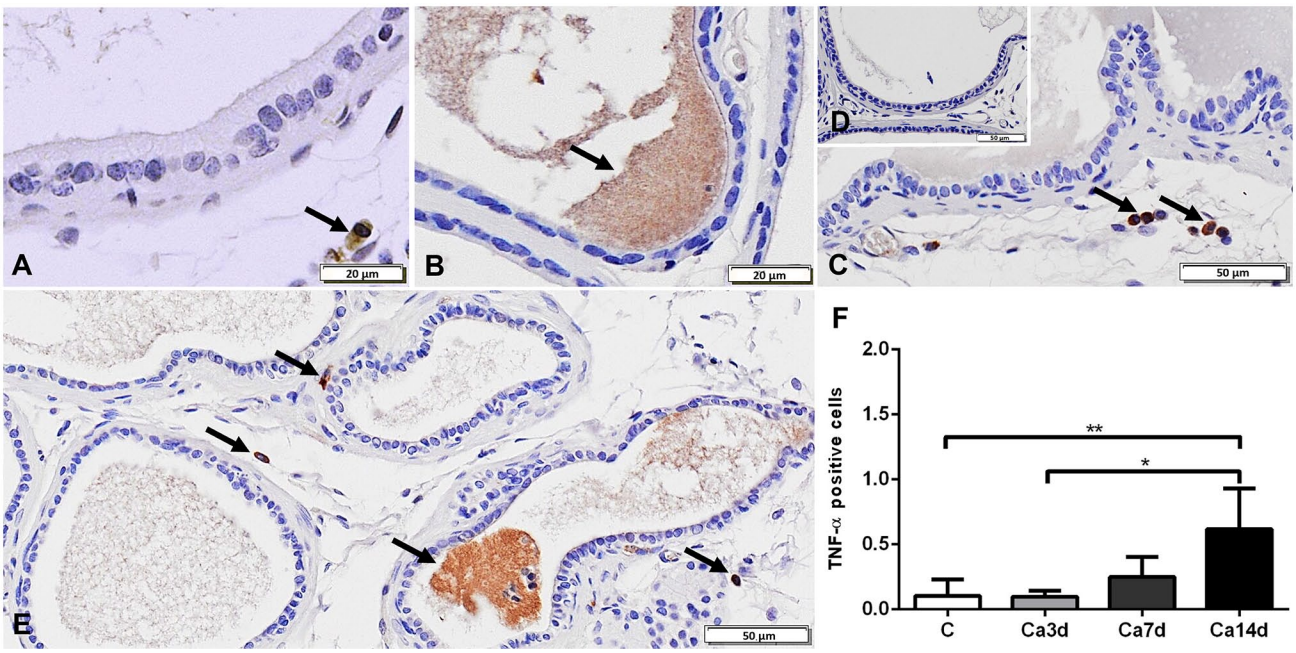

Figure 7. Surgical castration promotes an increase in TNF-α positive cells. Negative reaction control (D) slides were not incubated with primary antibody. Control (A), non-castrated animals. Castrated groups were euthanized at 3 (Ca3d) (B), 7 (Ca7d) (C, D), and 14 (Ca14d) (E) days after the orchiectomy. Immunoreactive cells are indicated by arrows. The data represents averages of the number of TNF-α positive cells by prostate area and the error bars show the standard deviation. * and ** indicate statistically significant differences ($p<0.05$ and $p<0.01$, respectively), according to the Kruskal-Wallis test followed by the post hoc Dunn test (F). Scale bar 50µm.

explained by an overexpression of receptors as an alternative to testosterone deficiency. The same occurs in castration-resistant prostate cancer cells, which, after androgen deprivation, employ various compensatory mechanisms such as gene amplification of AR and mutation of the genes of this receptor.[50] Furthermore, studies have shown that these cells can express cofactors that activate AR through non-canonical pathways, allowing independence from androgens.[51]

According to Justulin and collaborators (2010), the castration process causes the recruitment of macrophages and mast cells that contribute to the increase in MMPs.[52] These phagocytic cells also participate in regulation during the events of remodeling of the atrophic prostate.[52] These phagocytes are attracted due to androgen deprivation and participate in the process of prostatic tissue remodeling.[38,53] Macrophages are part of the phagocytic system and, in adult mammals, can be found in all tissues, exhibiting great morphological and functional diversity.[54] We observed an increase in Cd-68 positive cells in the prostatic intraepithelial region in the Ca3d group. Castration causes the loss of epithelial cells due to apoptosis,[18] especially in the first 72 hr[55] and these apoptotic cells express changes in the cell surface that allow recognition, phagocytosis, and removal by macrophages.[26,27] This removal occurs before cell lysis and prevents the release of intracellular toxins and apoptotic cell contents around the tissue, to avoid inflammation.[26,56–59] The apoptotic cells that are phagocytized by macrophages form vacuoles known as "autophagosomes" or "autophagy vacuoles." Some studies suggest that the formation of these vacuoles in the prostate epithelium leads to prostate atrophy after castration,[11,60–62] which may explain the increase in intraepithelial macrophages in the Ca3d group.

The results indicate that these phagocytes are also acting in the tissue reorganization of the prostate, since this cell type can secrete different chemical mediators and enzymes that actively participate in tissue remodeling, such as MMP-2 and MMP-9.[63,64] These enzymes are classified as gelatinases and play an important role in the degradation of the extracellular matrix during the tissue remodeling process,[65] such as after orchiectomy.[52,63] The MMPs are involved in the fibrillary collagen degradation process after the initial cleavage by collagenases.[65,66] Thus, the decrease in MMP-9 could be related to the increase in the relative volume of collagen in the Ca7d group.

The production and activation of MMPs depend on several factors and cytokines, such as TNF-α.[67,68] This protein is one of the main cytokines related to the regulation of the immune and inflammatory response.[69,70] TNF-α is produced by several cell types and is involved in the processes of apoptosis, cell differentiation, infiltration, and immune responses.[71,72] Studies reported the association of low testosterone concentration with increased serum levels of TNF-α in humans.[73–75] Based on this information, we believe that the period of testosterone deprivation influenced the increase in the frequency of TNF-α in the prostate of the Ca14d group in comparison to C and Ca3d. These results contribute to an increased understanding of the prostate remodeling process, considering the alterations that involve immune cells and components of the extracellular matrix caused by orchiectomy, a topic still underexplored in experimental models.

The results obtained here provide a better understanding of the cellular and tissue behavior that occurs in the prostate after orchiectomy. These data can help us better understand what happens in human prostate cancer after treatment with androgen deprivation, which in many cases can recur, generating castration-resistant cancer,[76] as well as better understand the behavior of immune cells, contributing to the advancement of the study of immunotherapies in the treatment of prostate cancer. The exploration of the mechanisms that lead to the changes observed in the prostate after castration is a limitation of the approach of the study; however, this does not compromise the conclusions obtained here, which can be evaluated infuturestudies.

Orchiectomy induces alterations in the prostatic architecture of gerbils, affecting the cellular arrangement and composition of the extracellular matrix. The results of the current study outline the tissue alterations observed after 3 days of androgen deprivation, highlighting the rapid response of the ventral prostate to hormonal fluctuations. The analysis of enzyme and cytokine expression, along with the characterization of the cellular microenvironment, aids in elucidating the mechanisms involved in post-orchiectomy tissue remodeling.

Acknowledgments

The authors thank MSc. Luiz Roberto Falleiros Junior for his technical assistance during the development of the experiments.

Competing Interests

The author(s) declared no potential conflicts of interest with respect to the research, authorship, and/or publication of this article.

Author Contributions

NFCC designed and performed the research, analyzed the data, and wrote the manuscript; VG analyzed the data and wrote the manuscript; CRSC performed the research and revised the manuscript; MIZ performed the research and revised the manuscript; SRT analyzed the data and revised the manuscript; and PSLV designed the research, analyzed the data, and wrote the manuscript.

Funding

The authors disclosed receipt of the following financial support for the research, authorship, and/or publication of this article: This work was financed by the National Council for Scientific and Technological Development—CNPq (Brazil) (Grant numbers 131528/2015-7 (NFCC); 141080/2024-8 (VG), 02938/2020-6 (SRT) 312111/2023-1 (PSLV)).

ORCID iDs

Nayara Fernanda Costa Castro https://orcid.org/0000-0002-8263-5223
Vitor Grigio https://orcid.org/0000-0002-6682-4550
Mariele Ilario Zucão https://orcid.org/0009-0007-2219-4984
Sebastião Roberto Taboga https://orcid.org/0000-0002-0970-4288
Patrícia Simone Leite Vilamaior https://orcid.org/0000-0001-9559-5497

Literature Cited

1. Aurich C. Castration. Encycl Reprod. 2018;1:165–70.
2. Malik R, Khan AP, Asangani IA, Cies¨ lik M, Prensner JR, Wang X, Iyer MK, Jiang X, Borkin D, Escara-Wilke J, Stender R, Wu YM, Niknafs YS, Jing X, Qiao Y, Palanisamy N, Kunju LP, Krishnamurthy PM, Yocum AK, Mellacheruvu D, Nesvizhskii AI, Cao X, Dhanasekaran SM, Feng FY, Grembecka J, Cierpicki T, Chinnaiyan AM. Targeting the MLL complex in castration-resistant prostate cancer. Nat Med. 2015;21(4):344–52.
3. Qi J, Fan L, Hussain A. Implications of ubiquitin ligases in castration-resistant prostate cancer. Curr Opin Oncol. 2015;27(3):172–6.
4. Bahmad HF, Jalloul M, Azar J, Moubarak MM, Samad TA, Mukherji D, Al-Sayegh M, Abou-Kheir W. Tumor microenvironment in prostate cancer: toward identification of novel molecular biomarkers for diagnosis, prognosis, and therapy development. Front Genet. 2021;12:652747.
5. Tsai YC, Chen WY, Abou-Kheir W, Zeng T, Yin JJ, Bahmad H, Lee YC, Liu YN, Androgen deprivation therapy-induced epithelial-mesenchymal transition of prostate cancer through downregulating SPDEF and activating CCL2. Biochim Biophys Acta Mol Basis Dis. 2018;1864(5, pt A):1717–27. doi:10.1016/j.bbadis.2018.02.016.
6. Alibhai SMH, Breunis H, Timilshina N, Naglie G, Tannock I, Krahn M, Warde P, Fleshner NE, Canning SD, Tomlinson G. Long-term impact of androgen-deprivation therapy on physical function and quality of life. Cancer. 2015;121(14):2350–7.
7. Meng MV, Grossfeld GD, Sadetsky N, Mehta SS, Lubeck DP, Carroll PR. Contemporary patterns of androgen deprivation therapy use for newly diagnosed prostate cancer. Urology. 2002;60(3, suppl 1):7–11.
8. Nishan U, da Rosa-Ribeiro R, Damas-Souza DM, Barbosa GO, Carvalho HF. Transcriptional regulators and regulatory pathways involved in prostate gland adaptation to a hypoandrogen environment. Genet Mol Biol. 2019;42(4):e20180362.
9. Perera M, Roberts MJ, Klotz L, Higano CS, Papa N, Sengupta S, Bolton D, Lawrentschuk N. Intermittent versus continuous androgen deprivation therapy in advanced prostate cancer. Curr Urol Rep. 2020;14(3):159–67.
10. Campos SG, Gonçalves BF, Scarano WR, Corradi LS, Santos FC, Custodio AM, Vilamaior PS, Góes RM, Taboga SR. Tissue changes in senescent gerbil prostate after hormone deprivation leads to acquisition of androgen insensitivity. Int J Exp Pathol. 2010;91(5):394–407.
11. Liu RF, Li J, Zhang J, Bai PD, Yang YF, Li W, Wu Z, Zheng JX. Crosstalk between apoptosis and autophagy in prostate epithelial cells under androgen deprivation. Exp Ther Med. 2018;15(3):2263–8.
12. Feng Q, He B. Androgen receptor signaling in the development of castration-resistant prostate cancer. Front Oncol. 2019;9:1–10.
13. Hsing AW, Reichardt JKV, Stanczyk FZ. Hormones and prostate cancer: current perspectives and future directions. Prostate. 2002;52(3):213–35.
14. Kyprianou N, Isaacs JT. Biological significance of measurable androgen levels in the rat ventral prostate following castration. Prostate. 1987;10(4):313–24.
15. Labrie F. Blockade of testicular and adrenal androgens in prostate cancer treatment. Nat Rev Urol. 2011;8(2):73–80.
16. Labrie F, Luu-The V, Bélanger A, Lin SX, Simard J, Pelletier G, Labrie C. Is dehydroepiandrosterone a hormone? J Endocrinol. 2005;187(2):169–96.
17. Zong Y, Goldstein AS. Adaptation or selection—mechanisms of castration-resistant prostate cancer. Nat Rev Urol. 2013;10(2):90–8.
18. Antonioli E, Della-Colleta HHM, Carvalho HF. Smooth muscle cell behavior in the ventral prostate of castrated rats. J Androl. 2004;25(1):50–6.
19. Vilamaior PS, Taboga SR, Carvalho HF. Modulation of smooth muscle cell function: morphological evidence for a contractile to synthetic transition in the rat ventral prostate after castration. Cell Biol Int. 2005;29(9):809–16.
20. Felisbino SL, Sanches BDA, Delella FK, Scarano WR, Dos Santos FCA, Vilamaior PSL, Taboga SR, Justulin LA. Prostate telocytes change their phenotype in response to castration or testosterone replacement. Sci Rep. 2019;9(1):1–12.
21. Oliveira SM, Vilamaior PSL, Corradi LS, Góes RM, Taboga SR. Cellular and extracellular behavior in the gerbil (Meriones unguiculatus) ventral prostate following different types of castration and the consequences of testosterone replacement. Cell Biol Int. 2007;31(3):235–45.
22. Kajiwara S, Ishii K, Sasaki T, Kato M, Nishikawa K, Kanda H, Arima K, Watanabe M, Sugimura Y. Castration-induced stromal remodeling disrupts the reconstituted prostate epithelial structure. Lab Invest. 2020;100(5):670–81.

23. Felisbino SL, Justulin Junior LA, Carvalho HF, Taboga SR. Epithelial-stromal transition of MMP-7 immunolocalization in the rat ventral prostate following bilateral orchiectomy. Cell Biol Int. 2007;31(10):1173–8.
24. Kurita T, Wang YZ, Donjacour AA, Zhao C, Lydon JP, O'Malley BW, Isaacs JT, Dahiya R, Cunha GR. Paracrine regulation of apoptosis by steroid hormones in the male and female reproductive system. Cell Death Differ. 2001;8(2):192–200.
25. Desai KV, Michalowska AM, Kondaiah P, Ward JM, Shih JH, Green JE. Gene expression profiling identifies a unique androgen-mediated inflammatory/immune signature and a PTEN (Phosphatase and tensin homolog deleted on chromosome 10)-mediated apoptotic response specific to the rat ventral prostate. Mol Endocrinol. 2004;18(12):2895–907.
26. Silva JAF, Bruni-Cardoso A, Augusto TM, Damas-Souza DM, Barbosa GO, Felisbino SL, Stach-Machado DR, Carvalho HF. Macrophage roles in the clearance of apoptotic cells and control of inflammation in the prostate gland after castration. Prostate. 2018;78(2):95–103.
27. Barbosa GO, Silva JAF, Siqueira-Berti A, Nishan U, Rosa-Ribeiro R, Oliveira SBP, Baratti MO, Ferrucci D, Santana JCO, Damas-Souza DM, Bruni-Cardoso A, Augusto TM, Corrêa-da-Silva F, Moraes-Vieira PM, Stach-Machado DR, Felisbino SL, Menezes GB, Cesar CL, Carvalho HF. Castration-induced prostate epithelial cell apoptosis results from targeted oxidative stress attack of M1142-macrophages. J Cell Physiol. 2019;234(10):19048–58.
28. Krolewski JJ, Singh S, Sha K, Jaiswal N, Turowski SG, Pan C, Rich LJ, Seshadri M, Nastiuk KL. TNF signaling is required for castration-induced vascular damage preceding prostate cancer regression. Cancers. 2022;14(24):6020. https://www.mdpi.com/2072-6694/14/24/6020.
29. Zhang R, Singh S, Pan C, Xu B, Kindblom J, Eng KH, Krolewski JJ, Nastiuk KL. Rate of castration-induced prostate stroma regression is reduced in a mouse model of benign prostatic hyperplasia. Am J Clin Exp Urol. 2023;11(1):12–26. http://www.ncbi.nlm.nih.gov/pubmed/36923722%0Ahttp://www.pubmedcentral.nih.gov/articlerender.fcgi?artid=PMC10009314.
30. Santos FCA, Rochel-Maia SS, Fochi RA, Justulin LA, Santos SAA, Vilamaior PSL, Felisbino SL, Góes RM, Taboga SR. MMP-2 and MMP-9 localization and activity in the female prostate during estrous cycle. Gen Comp Endocrinol. 2011;173(3):419–27. doi:10.1016/j.ygcen.2011.06.017.
31. Gonçalves BF, de Campos SG, Zanetoni C, Scarano WR, Falleiros LR Jr, Amorim RL, Góes RM, Taboga SR. A new proposed rodent model of chemically induced prostate carcinogenesis: distinct time-course prostate cancer progression in the dorsolateral and ventral lobes. Prostate. 2013;73(11):1202–3.
32. Guerra LHA, Tamarindo GH, de Campos SGP, Taboga SR, Vilamaior PSL. Do mineral and corn oil serve as potential endocrine disruptors in the gerbil prostate? Reprod Toxicol. 2019;90:141–9. doi:10.1016/j.reprotox.2019.09.004.
33. Maldarine JS, Sanches BDA, Santos VA, Amaro GM, Calmon MF, Rahal P, Góes RM, Vilamaior PSL, Taboga SR. Low-dose in utero exposure to finasteride promotes developmental changes in both male and female gerbil prostates. Environ Toxicol. 2020;35(1):15–26.
34. Sanches BDA, Carvalho HF, Maldarine JS, Biancardi MF, Santos FCA, Vilamaior PSL, Taboga SR. Differences between male and female prostates in terms of physiology, sensitivity to chemicals and pathogenesis—A review in a rodent model. Cell Biol Int. 2020;44(1):27–35.
35. Weibel ER. Principles and methods for the morphometric study of the lung and other organs. Lab Invest. 1978;12:131–55.
36. Huttunen E, Romppanen T, Helminen HJ. A histoquantitative study on the effects of castration on the rat ventral prostate lobe. J Anat. 1981;132(pt 3):357–70.
37. Varghese F, Bukhari AB, Malhotra R, De A. IHC profiler: an open source plugin for the quantitative evaluation and automated scoring of immunohistochemistry images of human tissue samples. PLoS ONE. 2014;9(5):e96801.
38. Bruni-Cardoso A, Augusto TM, Pravatta H, Damas-Souza DM, Carvalho HF. Stromal remodelling is required for progressive involution of the rat ventral prostate after castration: identification of a matrix metalloproteinase-dependent apoptotic wave. Int J Androl. 2010;33(5):686–95.
39. Corradi LS, Góes RM, Carvalho HF, Taboga SR. Inhibition of 5-??-reductase activity induces stromal remodeling and smooth muscle de-differentiation in adult gerbil ventral prostate. Differentiation. 2004;72(5):198–208.
40. Cordeiro RS, Scarano WR, Campos SG, Santos FC, Vilamaior PS, Góes RM, Taboga SR. Androgen receptor in the Mongolian gerbil ventral prostate: evaluation during different phases of postnatal development and following androgen blockage. Micron. 2008;39(8):1312–24.
41. Alukal JP, Lepor H. Testosterone deficiency and the prostate. Urol Clin North Am. 2016;43(2):203–8. doi:10.1016/j.ucl.2016.01.013.
42. Pejčić T, Tosti T, Tešić Ž, Milković B, Dragičević D, Kozomara M, Čekerevac M, Džamić Z. Testosterone and dihydrotestosterone levels in the transition zone correlate with prostate volume. Prostate. 2017;77(10):1082–92. https://onlinelibrary.wiley.com/doi/10.1002/pros.23365.
43. Prins GS, Birch L, Greene GL. Androgen receptor localization in different cell types of the adult rat prostate. Endocrinology. 1991;129(6):3187–99.
44. Vilamaior PSL, Felisbino SL, Taboga SR, Carvalho HF. Collagen fiber reorganization in the rat ventral prostate following androgen deprivation: a possible role for smooth muscle cells. Prostate. 2000;45(3):253–8.
45. Banerjee S, Banerjee PP, Brown TR. Castration-induced apoptotic cell death in the Brown Norway rat prostate decreases as a function of age. Endocrinology. 2000;141(2):821–32.
46. Yoon FH, Gardner SL, Danjoux C, Morton G, Cheung P, Choo R. Testosterone recovery after prolonged androgen suppression in patients with prostate cancer. J Urol. 2008;180(4):1438–43.
47. Husmann DA, Wilson CM, McPhaul MJ, Tilley WD, Wilson JD. Antipeptide antibodies to two distinct regions of the androgen receptor localize the receptor protein to

the nuclei of target cells in the rat and human prostate. Endocrinology. 1990;126(5):2359–68.
48. Prins GS, Putz O. Molecular signaling pathways that regulate prostate gland development. Differentiation. 2008;76(6):641–59.
49. Prins GS, Birch L. Immunocytochemical analysis of androgen receptor along the ducts of the separate rat prostate lobes after androgen withdrawal and replacement. Endocrinology. 1993;132(1):169–78.
50. Bahmad HF, Peng W, Zhu R, Ballout F, Monzer A, Elajami MK, Kobeissy F, Abou-Kheir W, Mechref Y. Protein expression analysis of an in vitro murine model of prostate cancer progression: towards identification of high-potential therapeutic targets. J Pers Med. 2020;10(3):1–19.
51. Daoud G, Monzer A, Bahmad H, Chamaa F, Hamdar L, Mouhieddine TH, Shayya S, Eid A, Kobeissy F, Liu YN, Abou-Kheir W. Primary versus castration-resistant prostate cancer: modeling through novel murine prostate cancer cell line. Oncotarget. 2016;7(20): 28961–75.
52. Justulin Jr LA, Della-Coleta HHM, Taboga SR, Felisbino SL. Matrix metalloproteinase (MMP)-2 and MMP-9 activity and localization during ventral prostate atrophy and regrowth. Int J Androl. 2010;33(5):696–708. https://onlinelibrary.wiley.com/doi/10.1111/j.1365-2605.2009.01016.x.
53. Rochel-Maia SS, Santos FC, Vilamaior PS, Justulin LA Jr, Felisbino SL, Góes RM, Taboga SR. MMP-2 and TIMP-2 in the prostates of male and female Mongolian gerbils: effects of hormonal manipulation. Histol Histopathol. 2011;26(11):1423–34.
54. Wynn TA, Chawla A, Pollard JW. Macrophage biology in development, homeostasis and disease. Nature. 2013;496(7446):445–55.
55. Buttyan R, Shabsigh A, Perlman H, Colombel M. Regulation of apoptosis in the prostate gland by androgenic steroids. Trends Endocrinol Metab. 1999;10(2):47–54.
56. Chawla A. Control of macrophage activation and function by PPARs. Circ Res. 2010;106(10):1559–69.
57. Fadok VA, Bratton DL, Konowal A, Freed PW, Westcott JY, Henson PM. Macrophages that have ingested apoptotic cells in vitro inhibit proinflammatory cytokine production through autocrine/paracrine mechanisms involving TGF-β, PGE2, and PAF. J Clin Invest. 1998;101(4):890–8.
58. Gordon S. Phagocytosis: an immunobiologic process. Immunity. 2016;44(3):463–75.
59. Gordon S. Alternative activation of macrophages. Nat Rev Immunol. 2003;3(1):23–35.
60. Helminen HJ, Ericsson JL. Ultrastructural studies on prostatic involution in the rat. Mechanism of autophagy in epithelial cells, with special reference to the rough-surfaced endoplasmic reticulum. J Ultrastruct Res. 1971;36(5):708–24.
61. Helminen HJ, Ericsson JL. Ultrastructural studies on prostatic involution in the rat. Evidence for focal irreversible damage to epithelium, and heterophagic digestion in macrophages. J Ultrastruct Res. 1972;39(5):443–55.
62. Kwong J, Choi HL, Huang Y, Chan FL. Ultrastructural and biochemical observations on the early changes in apoptotic epithelial cells of the rat prostate induced by castration. Cell Tissue Res. 1999;298(1):123–36.
63. Fang LY, Izumi K, Lai KP, Liang L, Li L, Miyamoto H, Lin WJ, Chang C. Infiltrating macrophages promote prostate tumorigenesis via modulating androgen receptor-mediated CCL4-STAT3 signaling. Cancer Res. 2013;73(18):5633–46.
64. Mantovani A, Sica A, Sozzani S, Allavena P, Vecchi A, Locati M. The chemokine system in diverse forms of macrophage activation and polarization. Trends Immunol. 2004;25(12):677–86.
65. Vihinen P, Ala-aho R, Kahari VM. Matrix metalloproteinases as therapeutic targets in cancer. Curr Cancer Drug Targets. 2005;5(3):203–20.
66. Santos SAA, dos Porto Amorim EM, Ribeiro LM, Rinaldi JC, Delella FK, Justulin LA, Felisbino SL. Hyperglycemic condition during puberty increases collagen fibers deposition in the prostatic stroma and reduces MMP-2 activity. Biochem Biophys Res Commun. 2017;493(4):1581–6. https://linkinghub.elsevier.com/retrieve/pii/S0006291X17319848.
67. Hagemann T, Robinson SC, Schulz M, Trümper L, Balkwill FR, Binder C. Enhanced invasiveness of breast cancer cell lines upon co-cultivation with macrophages is due to TNF-α dependent up-regulation of matrix metalloproteases. Carcinogenesis. 2004;25(8):1543–9.
68. Leber T, Balkwill FR. Regulation of monocyte MMPm9 production by TNF*a and a tumour-derived soluble factor (MMPSF). Br J Cancer. 1998;78:724–32.
69. Locksley RM, Killeen N, Lenardo MJ. The TNF and TNF receptor superfamilies: integrating mammalian biology. Cell. 2001;104(4):487–501.
70. Tian Y, Guo Y, Zhu P, Zhang D, Liu S, Tang M, Wang Y, Jin Z, Li D, Yan D, Li G, Zhu X. TRIM59 loss in M2 macrophages promotes melanoma migration and invasion by upregulating MMP-9 and Madcam1. Aging. 2019;11(19):8623–41.
71. Jia YL, Liu X, Yan JY, Chong LM, Li L, Ma AC, Zhou L, Sun ZY. The alteration of inflammatory markers and apoptosis on chronic prostatitis induced by estrogen and androgen. Int Urol Nephrol. 2015;47(1):39–46.
72. Luo Y, Yang P, Li Z, Luo Y, Shen J, Li R, Zheng H, Liang Y, Xia N. Liraglutide improves non-alcoholic fatty liver disease in diabetic mice by modulating inflammatory signaling pathways. Drug Des Devel Ther. 2019;13:4065–74.
73. Bobjer J, Katrinaki M, Tsatsanis C, Lundberg Giwercman Y, Giwercman A. Negative association between testosterone concentration and inflammatory markers in young men: a nested cross-sectional study. PLoS ONE. 2013;8(4):e61466.
74. Hotta Y, Kataoka T, Kimura K. Testosterone deficiency and endothelial dysfunction: nitric oxide, asymmetric dimethylarginine, and endothelial progenitor cells. Sex Med Rev. 2019;7(4):661–8.
75. Mohamad NV, Wong SK, Wan Hasan WN, Jolly JJ, Nur-Farhana MF, Ima-Nirwana S, Chin KY. The relationship between circulating testosterone and inflammatory cytokines in men. Aging Male. 2019;22(2):129–40.
76. Lu H, Teng Z, Wang J, Zhang W. Prostate cancer immunotherapy-based strategies: an updated review emphasizing immune checkpoint inhibitors. Front Immunol. 2025;16:1583363.